RSC Chemical Biology

ROYAL SOCIETY OF CHEMISTRY

PAPER

View Article Online
View Journal

Cite this: DOI: 10.1039/d6cb00107f

The position of hydrophobic residues impacts cellular uptake and intracellular localization of cell penetrating peptides

Adeline Schmitt and Helma Wennemers *

Received 20th March 2026,
Accepted 13th May 2026

DOI: 10.1039/d6cb00107f

rsc.li/rsc-chembio

Cell-penetrating peptides (CPPs) are widely used to deliver cargo into mammalian cells, yet efficient cellular uptake and endosomal escape remain key challenges. In this study, we evaluated how hydrophobic (4*S*)-4-cyclohexylproline (ChPro) residues and their spatial arrangement influence cellular uptake, endosomal escape, and subcellular distribution of conformationally constrained cationic peptides consisting of (4*S*)-guanidiniumproline (Gup). The evaluation revealed a greater effect on uptake and endosomal escape by positioning the hydrophobic block at the C- rather than the N-terminus. The amphipathic peptides with a C-terminal $(ChPro)_3$ sequence accumulated in mitochondria and the endoplasmic reticulum. These insights are relevant for optimizing cellular uptake, intracellular localization, and endosomal escape of CPPs.

Introduction

Cell-penetrating peptides (CPPs), short peptides that enter mammalian cells, are powerful tools for applications in drug delivery, gene therapy, and molecular imaging.[1–6] Their potency arises from their ability to deliver diverse molecular cargos, including small molecules,[7] nucleic acids,[8,9] and proteins.[10–12] However, efficient internalization, endosomal escape, and intracellular targeting are significant challenges.[13–16] Hydrophobic moieties facilitate interaction with the lipid bilayer and influence the properties of CPPs.[17–19] The insertion of hydrophobic residues into the lipid bilayer can enhance the translocation of peptides across the cell membrane. Accordingly, modulating the hydrophobic character of specific regions within a CPP can tune its properties.[18–29] The addition of hydrophobic moieties at the peptide termini has been shown to enhance cellular uptake, accelerate internalization, and, in some cases, promote endosomal escape.[17–19,24–26] The latter has been highlighted by Dowdy (Fig. 1A).[24] Futaki showed that a sequence of hydrophobic residues enables faster cellular uptake of octaarginine (R_8; Fig. 1B),[27,28] a sequence that Hackenberger showed is useful for protein delivery.[20–22] Furthermore, the strategic incorporation of tryptophan residues allowed for tuning of the uptake efficiency and internalization mechanism of oligoarginine peptides (Fig. 1C and D).[25,26] Furthermore, Raines showed how molecular cloaking of negative charge, *e.g.* carboxylates, enhances cellular uptake.[30]

Our group recently developed helical amphipathic proline-rich CPPs for mitochondria targeting.[29] In contrast to conformationally flexible oligoarginine peptides, these peptides adopt a rigid polyproline II (PPII)-helical conformation in which every third residue is stacked on top of another.[29,31,32] Previous studies had shown that octamers consisting exclusively of (4*S*)-guanidiniumproline (Gup, Z) internalize cells better than octaarginines and localize in the nucleoli.[32] The periodic implementation of (4*S*)-guanidiniumproline (Gup, Z) and cyclohexyl-containing residues at every third position (Fig. 1E, left) achieved helical CPPs with two cationic edges and one hydrophobic edge, which localize, particularly when a hydrophobic residue was placed at the C-terminus, in mitochondria.[29] Building on these findings, we investigated the role of hydrophobic tails on the behavior of cationic oligoproline-based CPPs. Here, we show that peptides with a block of hydrophobic residues at the C-terminus internalize more than analogs with hydrophobic residues at the N-terminus (Fig. 1E, right). Intracellular localization was observed not only at mitochondria, in the cytosol and the nuclei, but also in the endoplasmic reticulum (ER).

Laboratory of Organic Chemistry, ETH Zürich, D-CHAB, Vladimir-Prelog-Weg 3, Zürich 8093, Switzerland. E-mail: helma.wennemers@org.chem.ethz.ch

Experimental

Peptide synthesis, labeling and purification

Amino acid couplings. The peptides were synthesized manually by solid phase peptide synthesis (SPPS) using Rink Amide resin (0.67 mmol g^{-1}). For the coupling of secondary amines, Fmoc-Xaa-OH (3.0 eq.) and OxymaPure (3.0 eq.) were dissolved in a minimum of DMF/CH_2Cl_2 (1 : 1). DIC (6.0 eq.) was added, and the resulting solution was added to the amino-functionalized resin. The suspension was agitated for 2 h and then washed with DMF (3×). For the coupling of primary amines, Fmoc-Xaa-OH (3.0 eq.)

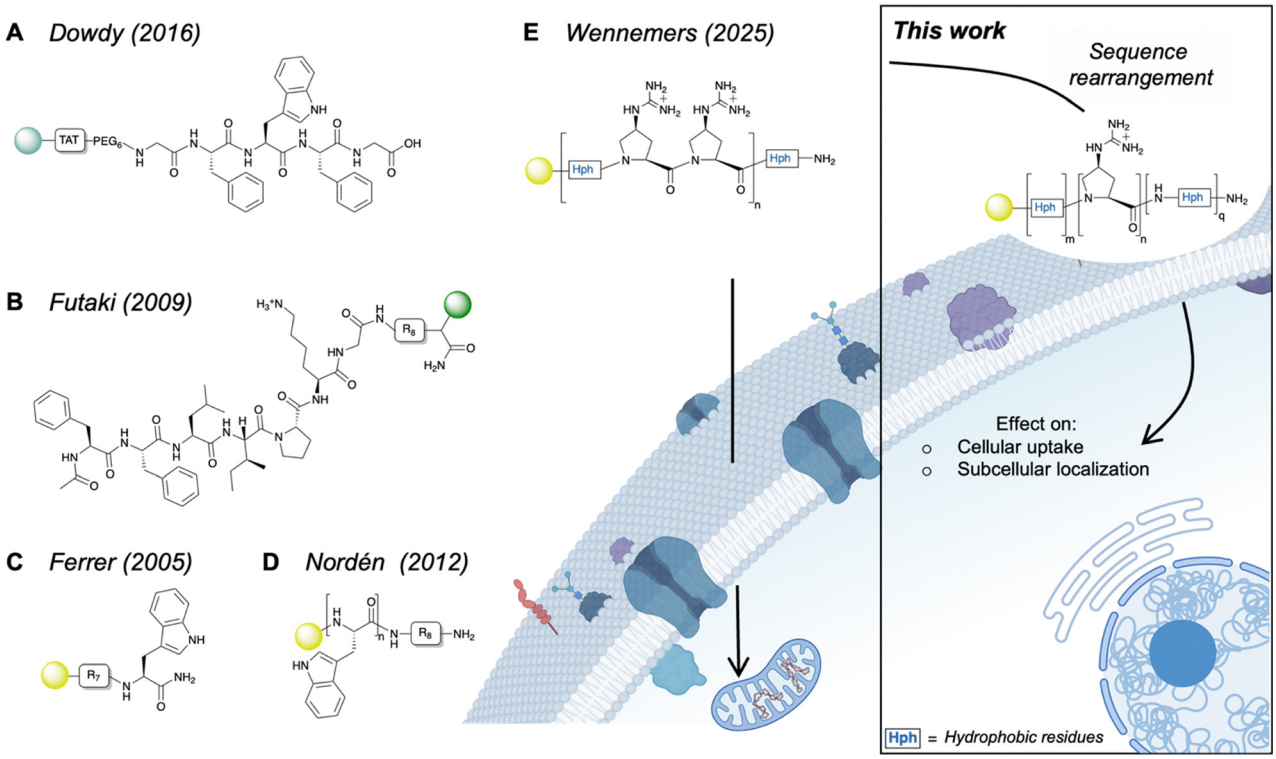

Fig. 1 Examples of cell penetrating peptides (CPPs) containing hydrophobic residues: (A) The -FWFG- sequence promotes endosomal escape of the TAT peptide.[24] (B) The -FFVIPKG- sequence accelerates the cellular uptake of R_8.[27] (C) Addition of W at the C-terminus of R_7 enhances uptake.[26] (D) Effect of W-content on cellular uptake of R_8.[25] (E) Left: PPII-helical amphipathic Gup-based oligoproline with periodically alternating residues, **$(ChProZZ)_2$-ChPro** targets mitochondria.[29] Right: PPII-helical peptides with hydrophobic residues at either the C- or the N- terminus. Dots correspond to the respective cargo: yellow, fluorescein; green, Alexa; grey, GFP β11 strand for split-GFP complementation assay. R = L-Arginine, TAT = TAT peptide, Hph = hydrophobic residue, m = 0–3, n= 4 or 6, q = 0–3. Of note, the arrows depict cellular entry but not a specific entry mechanism.

and HATU (3.0 eq.) were dissolved in a minimum of DMF. Hünig's base (6.0 eq.) was added, and the resulting solution was added to the amino-functionalized resin. The suspension was agitated for 60 min and washed with DMF (3×).

Fmoc-deprotection. The Fmoc group was removed by addition of a solution of 40% (v/v) piperidine in DMF to the resin followed by agitation for 5 min, and then an additional 10 min in a freshly added solution of 40% (v/v) piperidine in DMF, followed by extensive washing with DMF.

Labeling with carboxyfluorescein. 5(6)-Carboxyfluorescein (1.5 eq.), Pfp-OH (1.5 eq.) and EDC·HCl (1.5 eq.) were dissolved in a minimum of dry DMF and shaken for 30 min. The resulting solution and Hünig's base (6.0 eq.) were added to the resin-bound peptide bearing an N-terminal amine and the mixture was agitated for 4 h at rt in the dark.

Removal of side-chain protecting groups. The peptides were deprotected and cleaved from the resin by addition of a solution of TFA/TIS/H_2O (95 : 2.5 : 2.5), twice for 1 h. Both filtrates were collected and concentrated under a N_2 flow. Cold Et_2O was added, and the resulting suspension was centrifuged for 4 min at 1.9 rcf (repeated 2 more times). The peptides were then purified by RP-HPLC. The peptides were used as TFA salts.

The concentration of peptide stock solutions was determined by UV-vis by measuring the absorbance at 494 nm in PBS (pH 7.4), using a molar extinction coefficient of 65 000 M^{-1} cm^{-1}.

Circular dichroism (CD) spectroscopy

The secondary structure of the peptides was analyzed by recording CD spectra of 50 μM solutions in H_2O (pH 5.7) at 25 °C.

Cellular studies

Confocal microscopy. MCF-7 cells (purchased from the European Collection of Authenticated Cell Cultures) were seeded in a 8-μwell Ibidi plate at 25 000 cells per well in DMEM (100 μL, 10% FCS) and allowed to adhere overnight. The medium was removed and the cells were washed with PBS (200 μL, 1×) and incubated with the peptide solution at 20 μM, 10 μM, 5 μM, 2.5 μM or 1.25 μM in DMEM (200 μL, 1% FCS) for 1 h at 37 °C. Then, the medium was removed, and the cells were washed with PBS (200 μL, 2×). MitoTracker Deep Red was distributed at 20 nM in DMEM (200 μL, 1% FBS) and the cells were incubated at 37 °C for 25 min. Alternatively, ER-Red stain was distributed at 1 μM in DMEM (200 μL, 1% FBS) and the cells were incubated at 37 °C for 25 min. The medium was then removed, and the cells were washed with PBS (200 μL, 2×). Hoechst33342 was distributed at 2 μM in DMEM (200 μL, 1% FBS) and the cells were incubated at 37 °C for 5 min. The cells were then washed with PBS (200 μL, 2×), and FluoroBrite medium (200 μL) was added. The live cells were monitored by

confocal microscopy at 37 °C, 5% CO_2. For the cells subjected to a 24 h rest period, the FluoroBrite medium was exchanged for DMEM (200 μL, 10% FBS) after the initial imaging, and the cells were kept in this medium for 24 h. Due to strongly reduced signal of the ER-Red stain after 24 h in cells, the cells were incubated with the ER-Red stain at 1 μM for 25 min in DMEM (200 μL, 1% FBS). All cells were washed, the medium was then exchanged for FluoroBrite DMEM, and the cells were imaged again.

Flow cytometry. MCF-7 cells were seeded in a 24-well plate at 150 000 cells per well in DMEM (1 mL, 10% FCS), and allowed to adhere overnight. The medium was removed, the cells were washed with PBS (250 μL, 1×) and incubated with the peptide solution at 20 μM, 10 μM, 5 μM, 2.5 μM or 1.25 μM in medium (200 μL, 1% FCS) for 1 h at 37 °C. The medium was removed, and the cells were washed with PBS (250 μL, 2×). Trypsin (100 μL, 0.05%) was added, and the cells were incubated at 37 °C for 5 min. D-PBS with Mg^{2+} and Ca^{2+} (300 μL, 4 °C) was added, the cells were resuspended and centrifuged for 5 min at 0.4 rcf. The supernatant was carefully removed, and the cells were resuspended in PBS containing 1.5 μM PI and 2 mM EDTA (400 μL at 4 °C). The cells were added to flow cytometry tubes and kept on ice prior to analysis. Each sample contained approximately 10 000 cells and was analyzed in triplicate. Cells were gated according to PI staining to exclude cells with compromised membranes, ensuring that the analysis was restricted to cells with preserved membrane integrity. Each experiment was repeated three times.

Results and discussion

C-terminal hydrophobic blocks enhance the cellular uptake of amphipathic CPPs more than N-terminal hydrophobic blocks

We started by investigating the effect of a block of hydrophobic residues at the N- or C-terminus on the cell penetration of rigid cationic oligoproline-based peptides. Towards this goal, we appended three (4*S*)-4-cyclohexylproline (ChPro) residues to either terminus of a Gup tetramer (Fig. 2A, top). The choice of ChPro residues maintains PPII helicity, with the hydrophobic cyclohexyl groups pointing outward at distances that do not cause steric repulsion. In addition, peptides comprising Gup and ChPro are stable to proteolysis in cell lysates (Fig. S1).[29] 5(6)-carboxyfluorescein (CF) was positioned *via* an aminohexanoic acid (Ahx) spacer at the N-terminus to allow for monitoring. The properties of the resulting peptides with cationic and hydrophobic blocks CF-Ahx-Z_4ChPro$_3$-NH_2 and CF-Ahx-ChPro$_3Z_4$-NH_2

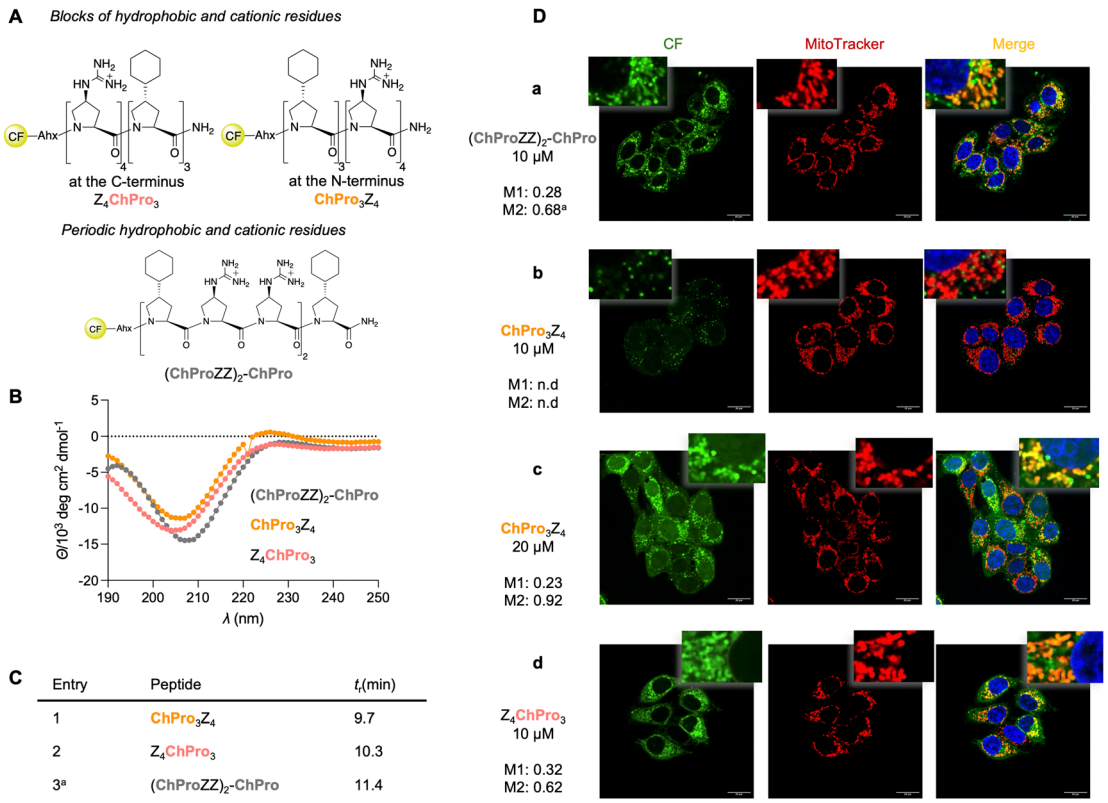

Fig. 2 (A) CPPs with blocks of hydrophobic and cationic residues (top) and periodically alternating residues (bottom); CF = 5(6)-Carboxyfluorescein, Ahx = aminohexanoic acid. (B) CD spectra, recorded at 50 μM in H_2O, pH 5.7. (C) Retention time of the CF-Ahx-peptides measured by RP-HPLC on a C4 column with a mobile phase from 30 to 55% of MeCN in H_2O/MeCN/TFA (1000/10/1) at 50 °C. (D) Representative confocal microscopic images of live MCF-7 cells, incubated for 1 h at 37 °C with peptide solutions (a)–(d) at their respective concentration in DMEM + 1% FBS (left, in green). Mitochondria were stained with MitoTracker Deep Red (middle, in red), and merged images (right, orange/yellow indicating colocalization) with Hoechst33342 stain for the nucleus (in blue), with respective Manders' coefficients: M1 corresponds to the fraction of peptide colocalizing with MitoTracker, and M2 to the fraction of MitoTracker colocalizing with the peptide. [a]Values from reference.[29] n.d. = not determined.

were compared with those of the constitutional isomer CF-Ahx-$(ChProZZ)_2$-ChPro-NH_2 (Fig. 2A, bottom). This amphiphilic reference peptide with periodically alternating ChPro and Gup (Z) residues was previously identified as a potent CPP that targets mitochondria.[29]

Circular dichroism (CD) analysis revealed that all peptides adopt a PPII helical conformation, characterized by a minimum between 203–208 nm and a maximum between 223–225 nm (Fig. 2B). The spectrum of **$(ChProZZ)_2$-ChPro** (Fig. 2B, grey) is slightly red-shifted relative to the spectra of the block peptides (Fig. 2B, orange and rose). Reverse phase high performance liquid chromatography (RP-HPLC) allows for an estimate of the hydrophobic character of the peptides. The three peptides eluted with retention times (t_r) between 9.7–11.4 min on a C4 column when using H_2O/MeCN/TFA (1000/10/1) and MeCN as mobile phases with a gradient of 30–55%. The retention time differences are small, but indicate that **$(ChProZZ)_2$-ChPro** (t_r = 11.4 min) is most hydrophobic, followed by **Z_4ChPro_3** (t_r = 10.3 min) and **$ChPro_3Z_4$** (t_r = 9.7 min) (Fig. 2C).

To investigate the cell penetrating properties, we incubated the peptides with breast cancer cells, MCF-7 cells, and used confocal microscopy to monitor their intracellular localization. The cells were incubated with the "block peptides" **Z_4ChPro_3** and **$ChPro_3Z_4$** at 5, 10, and 20 μM concentrations for 1 h (Fig. 2D and Fig. S2). MitoTracker Deep Red was added to stain mitochondria and Hoechst33342 for nuclei staining. At 10 μM, the reference peptide **$(ChProZZ)_2$-ChPro** localizes in mitochondria, the plasma membrane and endosomes (Fig. 2Da).[29] Confocal images show cytosolic punctuated fluorescence when peptide **$ChPro_3Z_4$** with the hydrophobic block at the N-terminus was incubated at 10 μM, suggesting that the peptide is predominantly trapped in endosomes (Fig. 2Db, Fig. S2 and S3). At higher concentration (20 μM), **$ChPro_3Z_4$** distributed through the cell, including the nucleus and mitochondria, with some remaining endosomal entrapment (Fig. S2Dc, S2 and S3).† Manders's coefficient analysis of MitoTracker with the CF fluorescence of **$ChPro_3Z_4$** revealed an M1 value of 0.23 and an M2 value of 0.92. This finding indicates that only a modest fraction of the peptide overlaps with MitoTracker (M1) and that the vast majority of mitochondrial signal contains peptide signal (M2). This pattern is consistent with a peptide that diffuses broadly throughout the cell but is nonetheless present at the majority of all mitochondrial sites.

With peptide **Z_4ChPro_3** that bears the hydrophobic block at the C-terminus, cellular uptake was observed starting at 10 μM (Fig. 2Dd and Fig. S2). In contrast to the isomeric CPPs, the confocal images show little punctuated fluorescence, indicating minimal to no endosomal entrapment. While the nucleus remained clear of the peptide, **Z_4ChPro_3** localized in mitochondria and, with a distinct pattern, around the nuclear membrane and in the cytosol. This pattern resembles the extensive, continuous membrane network of the endoplasmic reticulum (ER), which extends from the outer nuclear membrane throughout the cytoplasm. We therefore investigated colocalization of **Z_4ChPro_3** with mitochondria and the ER. For mitochondria, these analyses yielded M1 and M2 values of 0.32 and 0.62, respectively, indicating that a considerable fraction of mitochondria coincides with the peptide (M2), but only part of the peptide overlaps with the mitochondria (M1).

Incubation of MCF-7 cells with **Z_4ChPro_3** (10 μM, 1 h) followed by ER staining with ER-Red stain revealed colocalization (M1 = 0.80), suggesting that the observed fluorescence of **Z_4ChPro_3** around the nuclear membrane arises from ER localization (Fig. 3A). Owing to the close spatial proximity between mitochondria and ER, distinction between fluorescence in either of these organelles was challenging.

In our previous study, we observed a redistribution of amphipathic CPPs within cells over time.[29] We therefore examined

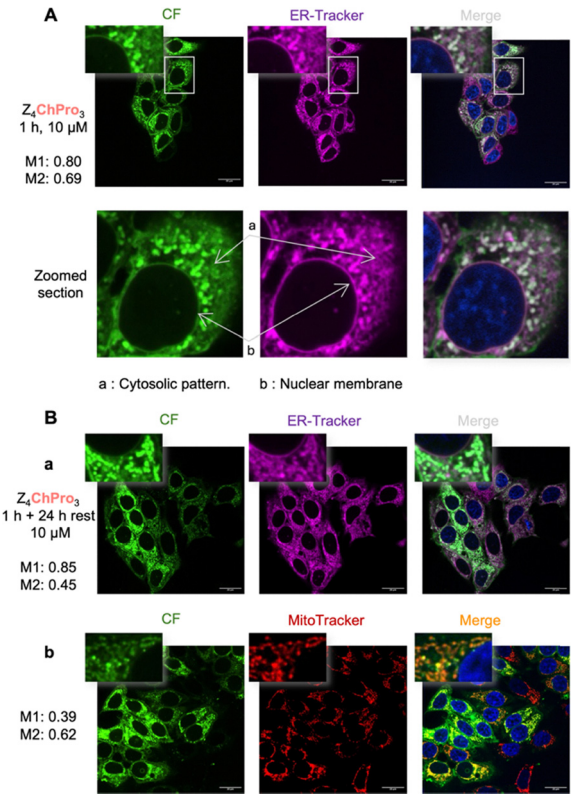

Fig. 3 (A) Representative confocal microscopic images of live MCF-7 cells, incubated for 1 h at 37 °C with Z_4ChPro_3 at 10 μM in DMEM + 1% FBS (left, in green). ER was stained with ER-Red stain (middle, in magenta), and merged images (right, white indicating colocalization) with Hoechst33342 stain for the nucleus (in blue). (B) Representative confocal microscopic images of live MCF-7 cells, incubated for 1 h at 37 °C with Z_4ChPro_3 at 10 μM in DMEM + 1% FBS, followed by a 24 h rest period in DMEM + 10% FCS (left, in green) with (a) ER-Red stain for staining of the ER (middle, in magenta), and merged images (right, white indicating colocalization); and (b) MitoTracker Deep Red for staining of mitochondria (middle, in red), and merged images (right, orange/yellow indicating colocalization); and Hoechst33342 stain for the nucleus (in blue). Manders' coefficients: M1 corresponds to the fraction of peptide colocalizing with the respective organelle, and M2 to the fraction of the organelle colocalizing with the peptide.

† Endosomes are acidic, which can affect the total fluorescence observed with fluorescein-labeled CPPs. Yet, spot-checks with related CPPs bearing rhodamine in place of fluorescein have yielded comparable relative cellular uptake.

whether mitochondrial and ER localization becomes more pronounced after prolonged incubation times. After 1 h incubation with the peptide, we therefore replaced the medium with DMEM supplemented with 10% FBS, incubated the cells for 24 h, and imaged them again (Fig. 3B). ER colocalization of the peptide remained comparable over time, with Manders M1 values of 0.80 after 1 h and 0.85 after a 24 h rest period (Fig. 3Ba).

In contrast, the fraction of ER signal overlapping with the peptide decreased over time, as reflected by a reduction in M2 from 0.69 at 1 h to 0.45 after the 24 h rest period. Mitochondrial colocalization remained rather constant over time (M1 = 0.32 and 0.39; M2 = 0.62) (Fig. 2Dd and 3Bb). Together, these results indicate that **Z_4ChPro$_3$** bearing hydrophobic residues at the C-terminus persists at mitochondria, while the association with the ER becomes less.

Cell viability was assessed by MTT assays (Fig. S4). After incubation of MCF-7 cells with the peptides for 1 h, **ChPro$_3$Z$_4$** did not exhibit toxicity at any tested concentration (5–20 μM), while **Z_4ChPro$_3$** caused a small reduction in viability at 10 μM (85%), and more significant cytotoxicity was observed at 15 μM and 20 μM, where viability decreased to 60% and 50%, respectively.

These results from the MTT assays are consistent with the appearance of the cells in confocal images (Fig. S2). Membrane integrity was further corroborated by incubating the cells with propidium iodide (PI), a membrane-impermeant nucleic acid stain (Fig. S5).

Next, we quantified the cellular uptake of the different peptides by flow cytometry. As for the confocal imaging studies, we incubated the peptides with MCF-7 cells for 1 h at 37 °C. Based on the observed cytotoxicity at higher concentrations, we only examined **Z_4ChPro$_3$** at concentrations of 5 and 10 μM (Fig. 4, rose, Fig. S2, S4 and S5). **ChPro$_3$Z$_4$** was examined at concentrations of 5, 10, 15 and 20 μM (Fig. 4, orange, Fig. S2, S4 and S5). Consistent with the confocal microscopy studies, the position of the hydrophobic tail impacted the overall uptake of the peptides. A C-terminal hydrophobic tail, as in **Z_4ChPro$_3$**, enhanced the cellular uptake by ~1.5-fold, both at 5 μM and 10 μM, in comparison to an N-terminal tail as in **ChPro$_3$Z$_4$** (Fig. 4, orange and rose). It is noteworthy that the uptake of **(ChProZZ)$_2$-ChPro** with a periodic arrangement of hydrophobic and cationic proline residues is still greater (Fig. 4, grey). This finding shows that the periodic pre-organization of the charges along the PPII helical scaffold enables higher delivery efficiency in comparison to isomers with cationic and hydrophobic blocks.‡

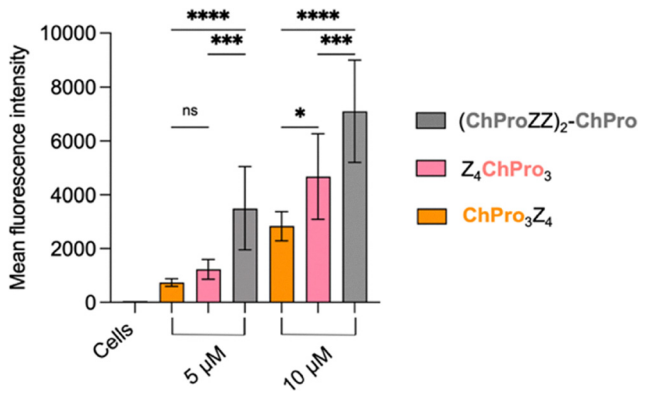

Fig. 4 Flow cytometry analyses after incubating MCF-7 cells for 1 h at 37 °C with the peptides at different concentrations. The indicated *P*-values were determined using one-way ANOVA followed by Tukey's multiple comparisons test per group of peptides (0.1234 (ns), 0.03328(*), 0.0021 (**), 0.0002 (***), <0.0001(****)).

The observed differences in intracellular localization prompted us to conduct initial experiments regarding the peptides' entry mechanism. Endocytosis is an energy-dependent entry pathway. We, therefore, compared the uptake of the peptides after 1 h incubation at 37 °C *versus* 4 °C.§ Flow cytometry analysis showed less uptake of both **Z_4ChPro$_3$** and **ChPro$_3$Z$_4$** after incubation at 4 °C (Fig. S6 and S7), consistent with a preference for an endocytic pathway. Whereas the confocal images show **ChPro$_3$Z$_4$** localized in endosomes, **Z_4ChPro$_3$** is not endosomally entrapped. This finding suggests that a C-terminal, but not an N-terminal, hydrophobic tail functions as an endosomal escape domain, enabling efficient release of the peptide into the cytosol.¶

Lastly, we evaluated whether the ChPro$_3$ motif promotes the uptake of other CPPs. As a model CPP, we chose the well-established cationic retro-TAT peptide (**rTAT**), which is easily prepared and derivatized *via* a glycine residue at the C-terminus (Fig. 5A). Cellular uptake studies at different concentrations followed by confocal imaging showed that a minimum concentration of 10 μM is required for detectable cellular internalization of the parent peptide **rTAT** (Fig. S8). In stark contrast, the analog bearing a C-terminal ChPro$_3$, **rTAT-ChPro$_3$** internalized at a concentration as low as 1.25 μM (Fig. 5Bb and Fig. S8). Both peptides distributed throughout the cytosol, with minimal punctuated fluorescence.

Neither peptide localized at the mitochondria nor accumulated specifically at the ER (Fig. 5B and Fig. S8). The absence of cytoplasmic puncta and enhanced uptake at lower concentration in the case of **rTAT-ChPro$_3$** implies enhanced endosomal escape through the hydrophobic block (Fig. 5Bb).‖ Flow cytometry studies confirmed the significantly greater overall cellular uptake of **rTAT-ChPro$_3$** compared to **rTAT** (Fig. 5C and Fig. S9, S10). The ChPro$_3$ sequence enhanced the cellular uptake by a remarkable 10-fold and 20-fold at 1.25 and 2.5 μM, respectively.

‡ Positioning ChPro$_3$ at the C-terminus leads to uneven CPP uptake, as also observed on the cytogram of flow cytometry analyses. (Fig. S7).

§ Of note, the comparison of cellular entry at 4 °C *versus* 37 °C provides basic insight into how a compound enters cells, but does not elucidate the exact entry mechanism.

¶ Of note, the N-terminal fluorophore can, as a hydrophobic moiety, affect the cellular uptake.

‖ At concentrations of 5 μM or higher, rTAT-ChPro$_3$ altered the cellular morphology indicative of cytotoxicity (Fig. S17).

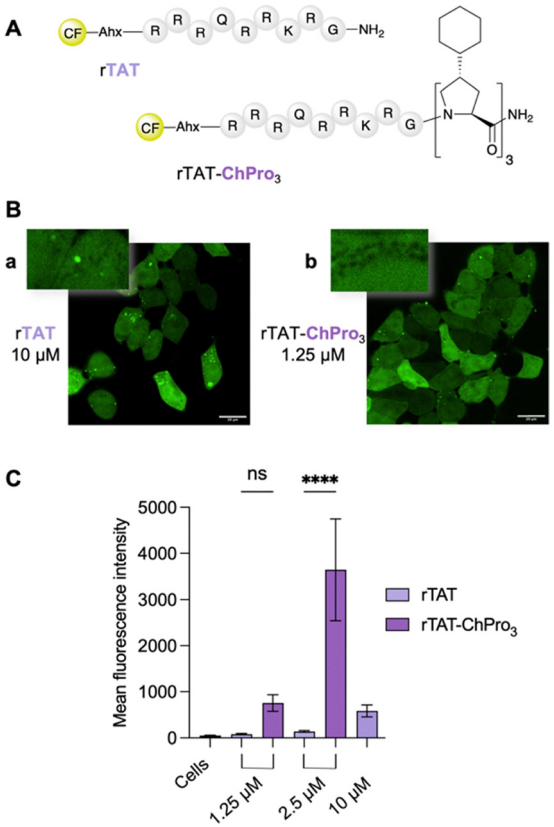

Fig. 5 (A) Peptides, rTAT and rTAT-ChPro$_3$; CF = 5(6)-Carboxyfluorescein, Ahx = aminohexanoic acid. (B) Representative confocal microscopic images of live MCF-7 cells, incubated for 1 h at 37 °C with peptide solutions (a) and (b) at their respective concentration in DMEM + 1% FBS (left, in green). ER was stained with ER-Red stain (middle, in magenta), and merged images (right, white indicating colocalization) with Hoechst33342 stain for the nucleus (in blue). (C) Flow cytometry analyses after incubating MCF-7 cells for 1 h at 37 °C with the peptides at different concentrations. The indicated *P*-values were determined using one-way ANOVA followed by Tukey's multiple comparisons test per group of peptides (0.1234 (ns), 0.03328(*), 0.0021 (**), 0.0002 (***), <0.0001(****)).

Conclusions

In conclusion, a hydrophobic tail composed of three ChPro residues enhances the uptake efficiency and influences the subcellular localization of cationic CPPs. Our studies on conformationally constrained peptides with four Gup residues showed that a C-terminal ChPro$_3$ tail enhances internalization more than an N-terminal ChPro$_3$ tail. The C-terminal hydrophobic block (**Z$_4$ChPro$_3$**) enabled targeting of mitochondria and the ER. N-terminal hydrophobic residues promote uptake, mitochondria accumulation, and distribution throughout the cell, but only at higher concentrations. At either terminus, the ChPro$_3$ motif facilitates endosomal escape and release of the CPP into the cytosol, with a significantly greater effect when localized at the C-terminus. Studies with the retro-TAT peptide underscored the general applicability of the ChPro$_3$ motif for enhanced uptake and endosomal release. Since many therapeutic targets are localized in the cytosol, high cellular uptake combined with endosomal escape is critical for cargo delivery. We therefore anticipate the ChPro$_3$ motif to be a useful tool for intracellular delivery.

Author contributions

Conceptualization and writing, A.S and H.W; investigation, A.S.

Conflicts of interest

There are no conflicts to declare.

Data availability

All data are available in the manuscript or the accompanying supplementary information (SI). Supplementary information: general aspects and materials, details on experimental procedures, compound characterization, additional data on the cellular uptake, toxicity and stability. See DOI: https://doi.org/10.1039/d6cb00107f.

Acknowledgements

We thank Leyla Hernandez for contributions to cell culture. We acknowledge the Scientific Center for Optical and Electron Microscopy (ScopeM), the Flow Cytometry Core Facility (FCCF) and the Molecular and Biomolecular Analysis Service (MoBiAS) of ETH Zürich for support. We thank ETH Zurich for funding this research. Fig. 1 was created in BioRender. Schmitt, A. (2026): https://BioRender.com/aum3n7lr.

Notes and references

1 F. Heitz, M. C. Morris and G. Divita, *Br. J. Pharmacol.*, 2009, **157**, 195–206.
2 A. D. Frankel and C. O. Pabo, *Cell*, 1988, **55**, 1189–1193.
3 M. Green and P. M. Loewenstein, *Cell*, 1988, **55**, 1179–1188.
4 E. G. Stanzl, B. M. Trantow, J. R. Vargas and P. A. Wender, *Acc. Chem. Res.*, 2013, **46**, 2944–2954.
5 A. Gori, G. Lodigiani, S. G. Colombarolli, G. Bergamaschi and A. Vitali, *ChemMedChem*, 2023, **18**, e202300236.
6 F. Madani, S. Lindberg, Ü. Langel, S. Futaki and A. Gräslund, *J. Biophys.*, 2011, **2011**, 414729.
7 A. F. L. Schneider, J. Kallen, J. Ottl, P. C. Reid, S. Ripoche, S. Ruetz, T. M. Stachyra, S. Hintermann, C. E. Dumelin, C. P. R. Hackenberger and A. L. Marzinzik, *RSC Chem. Biol.*, 2021, **2**, 1661–1668.
8 I. Nakase, H. Akita, K. Kogure, A. Gräslund, U. Langel, H. Harashima and S. Futaki, *Acc. Chem. Res.*, 2012, **45**, 1132–1139.
9 P. Boisguérin, S. Deshayes, M. J. Gait, L. O'Donovan, C. Godfrey, C. A. Betts, M. J. Wood and B. Lebleu, *Adv. Drug Delivery Rev.*, 2015, **87**, 52–67.
10 N. Nischan, H. D. Herce, F. Natale, N. Bohlke, N. Budisa, M. C. Cardoso and C. P. Hackenberger, *Angew. Chem., Int. Ed.*, 2015, **54**, 1950–1953.

11 M. Akishiba, T. Takeuchi, Y. Kawaguchi, K. Sakamoto, H. H. Yu, I. Nakase, T. Takatani-Nakase, F. Madani, A. Gräslund and S. Futaki, *Nat. Chem.*, 2017, **9**, 751–761.
12 W. Xiao, W. Jiang, Z. Chen, Y. Huang, J. Mao, W. Zheng, Y. Hu and J. Shi, *Signal Transduction Target Ther.*, 2025, **10**, 74.
13 S. Reissmann, *J. Pept. Sci.*, 2014, **20**, 760–784.
14 D. Pei and M. Buyanova, *Bioconjugate Chem.*, 2019, **30**, 273–283.
15 D. J. Brock, H. M. Kondow-McConaghy, E. C. Hager and J.-P. Pellois, *Bioconjugate Chem.*, 2019, **30**, 293–304.
16 S. Futaki, J. V. V. Arafiles and H. Hirose, *Chem. Lett.*, 2020, **49**, 1088–1094.
17 S. Pujals, J. Fernandez-Carneado, M. J. Kogan, J. Martinez, F. Cavelier and E. Giralt, *J. Am. Chem. Soc.*, 2006, **128**, 8479–8483.
18 J. Allen and J. P. Pellois, *Sci. Rep.*, 2022, **12**, 15981.
19 M. Oba, S. Nakajima, K. Misao, H. Yokoo and M. Tanaka, *Bioorg. Med. Chem.*, 2023, **91**, 117409.
20 A. F. L. Schneider, M. Kithil, M. C. Cardoso, M. Lehmann and C. P. R. Hackenberger, *Nat. Chem.*, 2021, **13**, 530–539.
21 J. V. V. Arafiles, J. Franke, L. Franz, J. Gómez-González, K. Kemnitz-Hassanin and C. P. R. Hackenberger, *J. Am. Chem. Soc.*, 2023, **145**, 24535–24548.
22 J. Franke, J. V. V. Arafiles, C. Leis and C. P. R. Hackenberger, *Angew. Chem., Int. Ed.*, 2025, **64**, e202506802.
23 S. Tamura, G. Tsuji and Y. Demizu, *Bioorg. Med. Chem.*, 2025, **126**, 118223.
24 P. Lönn, A. D. Kacsinta, X. S. Cui, A. S. Hamil, M. Kaulich, K. Gogoi and S. F. Dowdy, *Sci. Rep.*, 2016, **6**, 32301.
25 H. A. Rydberg, M. Matson, H. L. Amand, E. K. Esbjörner and B. Nordén, *Biochemistry*, 2012, **51**, 5531–5539.
26 J. R. Maiolo, M. Ferrer and E. A. Ottinger, *Biochim. Biophys. Acta*, 2005, **1712**, 161–172.
27 K. Takayama, I. Nakase, H. Michiue, T. Takeuchi, K. Tomizawa, H. Matsui and S. Futaki, *J. Controlled Release*, 2009, **138**, 128–133.
28 K. Takayama, H. Hirose, G. Tanaka, S. Pujals, S. Katayama, I. Nakase and S. Futaki, *Mol. Pharm.*, 2012, **9**, 1222–1230.
29 A. Schmitt and H. Wennemers, *ACS Chem. Biol.*, 2025, **20**, 2298–2307.
30 K. A. Mix, J. E. Lomax and R. T. Raines, *J. Am. Chem. Soc.*, 2017, **139**, 14396–14398.
31 M. Kuemin, S. Schweizer, C. Ochsenfeld and H. Wennemers, *J. Am. Chem. Soc.*, 2009, **131**, 15474–15482.
32 Y. A. Nagel, P. S. Raschle and H. Wennemers, *Angew. Chem., Int. Ed.*, 2017, **56**, 122–126.